

# Molecular Dynamics Study of Interfacial Confinement Effects of Aqueous NaCl Brines in Nanoporous Carbon<sup>†</sup>

Matthew C. F. Wander and Kevin L. Shuford\*

Department of Chemistry, Drexel University, Philadelphia, Pennsylvania 19104

Received: May 31, 2010; Revised Manuscript Received: July 23, 2010

In this paper, studies of aqueous electrolyte solutions in contact with a family of porous carbon geometries using classical molecular dynamics simulations are presented. These simulations provide an atomic scale depiction of ion transport dynamics in different environments to elucidate power of aqueous electrolyte supercapacitors. The electrolyte contains alkali metal and halide ions, which allow for the examination of size trends within specific geometries as well as trends in concentration. The electrode pores are modeled as planar graphite sheets and carbon nanotubes with interstices ranging from one to four nanometers. Ordered layers form parallel to the carbon surface, which facilitates focused ion motion under slightly confining conditions. As a result, the ion's diffusivities are enhanced in the direction of the slit or pore. Further confining the system leads to decreased ion diffusivities. The ions are fully hydrated in all but the smallest slits and pores with those sizes showing increased ion pairing. There is strong evidence of charge separation perpendicular to the surface at all size scales, concentrations, and ion types, providing a useful baseline for examining differential capacitance behavior and future studies on energy storage. These systems show promise as high-power electrical energy storage devices.

## Introduction

The need for efficient electrical energy storage devices is an ever increasing component of modern society. With the advent of alternative energy sources, such as wind and solar that do not generate power on demand, that need is ever more acute. An inexpensive means of energy storage with high power and energy density characteristics is essential to the success of alternative energy generation technologies. Traditional technologies group storage devices into two categories: batteries, which have high-energy storage capabilities, and capacitors, which have higher delivery rates. Recent focus has been on supercapacitors, which show great promise as systems that combine both high power and large energy storage capabilities.

Nanoporous, carbon-based supercapacitors have received significant attention in recent years as potential energy storage devices.<sup>1–8</sup> Nanofibers are of particular interest for their high surface area and short diffusion distance.<sup>9</sup> One reason for the appeal of nanostructures is the ability to shape the carbon into nearly any morphology.<sup>10</sup> A second reason is that these systems can maintain nearly constant capacitance per unit area for pores as small as 1 nm.<sup>11</sup>

Ionic liquids display a wide variety of mechanisms for infiltration of nanoporous environments,<sup>12</sup> and infiltration is a potential issue when dealing with confined spaces. Certain ionic liquid supercapacitors can demonstrate an anomalously high capacitance when the pore size is approximately equal to the ion size.<sup>13,14</sup> This increase in capacitance has been observed in molecular dynamics simulations as well.<sup>15</sup>

Aqueous electrolyte supercapacitors have received less attention than ionic liquids or molten salts.<sup>16</sup> Their advantage is lower impedance and high power resulting from low viscosity of the brine.<sup>16</sup> The primary disadvantage of an aqueous electrolyte supercapacitor is the limitation of the electric

potential to  $\sim 1$  V.<sup>17</sup> Atomic scale determination of the properties of these systems is necessary because continuum models fail to correctly incorporate the drag effect of the fluid.<sup>18</sup>

The infiltration mechanism and flow characteristics of aqueous brines in carbon nanostructures are important properties that require careful examination. For pure water systems with small diameter nanopores, additional pressure is required for the water to infiltrate the pore.<sup>9</sup> The smaller the pore diameter, the higher the pressure required.<sup>19</sup> This applied pressure is also required for brines, where it has been found that the smaller the ion, the greater the induced pressure required.<sup>20</sup> Moreover, one must consider the potential for precipitation and clogging. At the smallest of the channels, there is a significant drop in solubility ( $\sim 7.4$  Å tube diameter).<sup>20</sup> Additionally, confinement can enhance other causes of ion pairing, such as those that result from the presence of a hydrophobic impurity like methane.<sup>21</sup>

Water dynamics in confined nanopore environments has also been of interest. It was reported that water in a tube did not demonstrate a unified flow when a potential gradient was induced, but rather diffusion was the dominant process.<sup>22</sup> In addition, studies of water adsorbed into nanotubes showed a strong hysteresis indicating that the internal structure of the water plays a more significant role in its behavior than interaction with the tube.<sup>23</sup> In very small donut-shaped nanotubes, water can form independent oppositely polarized chains, which can repulse one another.<sup>24</sup>

Ionic pairing and transport has also been of interest in confined pores.<sup>25–27</sup> In silica slit pores, hydration has been shown to control the behavior of ions.<sup>28</sup> It was also shown using silica nanopores that hydrophilicity and hydrophobicity will have a significant effect on diffusion.<sup>29</sup> In addition, surface roughness can alter substantially diffusion behavior.<sup>30</sup> While there is not expected to be site specific interactions with carbon, the confinement will cause a structuring of the water layer. This structuring can lead to indications of differential capacitance behavior, which for aqueous systems is likely to be a minimum

<sup>†</sup> Part of the "Mark A. Ratner Festschrift".

\* To whom correspondence should be addressed.

**TABLE 1: Atomic Parameters for Models Used in the Simulations**

system	$X/\text{\AA}$	$Y/\text{\AA}$	$Z/\text{\AA}^a$	no. of carbon atoms	no. of water molecules	no. of Na and Cl ions
1 nm slit	54.26	55.53	27.16	6864	555	10
1.5 nm slit	29.67	29.67	29.67	4300	555	10
2.5 nm slit	29.67	29.97	37.78	2016	555	10
4 nm slit	24.67	21.37	56.67	1200	555	10
4 nm slit 0.5 M	24.37	21.11	57.29	1200	555	5
4 nm slit 2 M	24.40	21.13	56.36	1200	555	20
4 nm slit 4 M	24.41	21.14	56.39	1200	555	40
bulk 0.5 M	22.83	20.72	36.40	0	555	5
bulk 1 M	22.83	20.75	36.42	0	555	10
bulk 2 M	23.14	21.03	36.76	0	555	20
bulk 4 M	23.39	21.26	37.32	0	555	40
1 nm nanotube	40.00	40.00	371.39	5436	555	10
1.5 nm nanotube	40.00	40.00	157.41	3072	555	10
2.5 nm nanotube	60.00	60.00	51.65	1596	555	10
3.5 nm nanotube	60.00	60.00	22.14	972	555	10

<sup>a</sup>This is the direction perpendicular to the slab or along the length of the tube.

with no surface charging.<sup>31</sup> While chemically similar to sodium, potassium has been shown to possess a strong capacitance profile within the electrical double layers of meso/micropores.<sup>32</sup>

In this study, classical molecular dynamics (MD) was used to determine the qualitative properties of an aqueous NaCl brine in contact with nanopores of carbon electrodes. Two different model pore geometries were examined, planar slits and cylindrical pores. The effect of changing concentration was also investigated with a deliberate focus on sodium chloride because of its ubiquity. This approach focuses on the calculation of atomic scale properties that contribute to bulk characteristics such as ion pairing and diffusivity constants rather than bulk scale properties such as power and capacitance. This approach will allow us to observe primary trends with changes of the brine composition, revealing sufficient information to determine which of these systems are suitable for experimental study and ultimately development as an energy storage technology.

## Methods

This is a classical molecular dynamics study using the program LAMMPS.<sup>33</sup> The time step for all MD simulations was 1 fs. Long-range sums were computed using the Ewald method as implemented in LAMMPS.<sup>34</sup> First, brines were equilibrated separately for up to 0.5 ns. During this run, the box would deform to fit the appropriate gap corresponding to the slit or pore of interest. These reshaped boxes were then placed into the appropriate carbon structure, which had been created separately in Materials Studio.<sup>35</sup> In all cases, the width of the slit or diameter of the pore was defined by the carbon-to-carbon gap size. The simulation boxes used in all cases were periodic in three dimensions. For the nanotubes, this was equivalent to a one-dimensional periodicity in the  $z$ -direction as the vacuum gap was greater than or equal to 2 nm in the  $x$ - and  $y$ -directions.

**Brine Selection.** NaCl (1 M) in a 4 nm slit pore was used as a baseline for the other simulations. These are pore concentrations only. No attempt has been made to connect to a possible surrounding bulk medium, as the focus was on the chemistry deep within the pore. The 1 M NaCl solution was examined in slits with 4, 2.5, 1.5, and 1 nm dimensions and tubes of 3.5, 2.5, 1.5, and 1 nm. In the 4 nm slit, other concentrations of NaCl were examined including 0, 0.5, 2, and 4 M. Table 1 summarizes the simulation boxes and their contents.

**TABLE 2: Force Field Parameters**

element	mass/AMU	charge/ $e^-$	
graphite C	12.011	0.00	
water O	15.9994	0.82	
water H	1.00797	0.41	
Na	22.99	1.00	
Cl	35.453	-01.00	
Lennard-Jones 12-6		pair coefficients	
parameters	$\epsilon/\text{kcal mol}^{-1}$	$\sigma/\text{\AA}$	
graphite C	0.1200	3.2963	
water O	0.1554	3.1655	
water H	0.0000	0.0000	
Na	0.1301	2.3502	
Cl	0.1000	4.4000	
bond coefficients			
	$\text{k/kcal \AA}^{-1}$	$r_0/\text{\AA}$	
graphite C-C	469.0	1.4	
water O-H	554.135	1.0	
angle coefficients			
	$\text{k/kcal } \theta^{-1}$	$r_0/\theta$	
graphite C-C-C	85.0	120.0	
H-O-H	45.7696	109.47	
dihedral coefficients			
	$\text{k/kcal } \varphi^{-1}$	phase	angular freq.
graphite C-C-C-C	5.3	-1	2

**Slit Pore Simulations and Analysis on Bulk Brines.** First, a 100 ps equilibration NVT (NVT: constant number, volume, and temperature) was run where the temperature was gradually adjusted from 0 to 300 K. Then a 200 ps NPT (NPT: constant number, pressure, and temperature) simulation was performed at 0 GPa ( $P \sim 1$  bar within simulation uncertainties) and 300 K. While all three boundaries were allowed to vary, the rigidity of the carbon sheets prevented significant variation in the  $x$ - and  $y$ -directions. This permitted the water in the simulation cell to reach a density appropriate to the surface conditions. Finally a 2 ns NVT ( $T = 300$  K) run was performed, where position data was sampled (every 1 ps) and analysis performed. During this portion of the simulation the carbon atoms were frozen.<sup>36</sup> For all simulations, long-range sums were computed using the Ewald method as implemented in LAMMPS.

**Cylindrical Pore Simulations.** Use of pressure equilibration was not feasible with the simulation design. As a result, instead of the NVT/NPT equilibration combination, 600 ps of NVT was used, first scaling up the temperature from 0 to 300 K over 200 ps followed by 400 ps at 300 K. The same 2 ns sampling run used in the slit case followed.

**Force Fields.** The force field for the aqueous brine was taken from ClayFF.<sup>37</sup> The ClayFF force field uses the flexible, single-point charge (SPC-Fw) water molecule. The carbon force field parameters were taken from the original Amber force field set.<sup>38</sup> All parameters have been summarized in Table 2.

**Analysis Methods.** The analysis of the radial distribution profiles (RDF) used to compute primary hydration shells was performed in LAMMPS. However, most of the analysis was post processed using a variety of code tools. A separate code was used to determine the atomic density profile perpendicular to the surface (vertical) from the trajectory files and was modified for this paper in order to create cylindrical profiles for the nanotubes.<sup>39</sup> An additional code was developed to calculate the conductivities and diffusivities, which are inherently connected

through the calculation of the mean-squared displacement of ions. For diffusivity constants ( $D_0$ ), the formula is

$$D_0 = \lim_{t \rightarrow \infty} \left( \frac{\langle \text{MSD}(t) \rangle}{nt} \right) \quad (1)$$

where  $\text{MSD}(t)$  is the time average of the mean squared displacement of a given species,  $t$  is time, and  $n$  is a constant that represents the confinement of the system. For bulk  $n = 6$ , for planar slits with 2 dimensions of freedom  $n = 4$ , and for the nanotubes with one dimension of freedom  $n = 2$ . From the diffusivities, the ideal- or diffusion-based charge transfer can be calculated as<sup>40</sup>

$$\lambda_{\text{ideal}} = \frac{e^2}{ntVk_{\text{B}}T} (n_i D_{0i} + n_j D_{0j}) \quad (2)$$

where  $t$  and  $n$  have the same meaning as in eq 1,  $V$  is the volume of the simulation box,  $T$  is temperature in Kelvin,  $k_{\text{B}}$  is Boltzman's constant,  $e$  is the fundamental charge of the electron,  $i$  denotes the cations,  $j$  denotes the anions, and  $n_i$  and  $n_j$  are the number of cations and anions in the system, respectively. Over a 2 ns period the diffusivities are quite stable, and the methodological error bars are smaller than the points on the graph. This expression is a useful upper bound to the available conductivity in the system. The formula to describe the correlation of the conductivity is<sup>40</sup>

$$\lambda_{\text{corr}} = \lim_{t \rightarrow \infty} \left( \frac{e^2}{ntVk_{\text{B}}T} \sum_{ij} z_i z_j \langle (\bar{\mathbf{R}}_i(t) - \bar{\mathbf{R}}_i(0)) \cdot (\bar{\mathbf{R}}_j(t) - \bar{\mathbf{R}}_j(0)) \rangle \right) \quad (3)$$

where  $z$  is the formal charges of the ion in atomic units,  $\mathbf{R}$  is the position vector of each atom, and the other variables have the same meanings as eqs 1 and 2. The difference between eqs 2 and 3 is defined here as the uncorrelated conductivity. The error in the correlation is reported as the standard deviation of the slope of  $\lambda$  versus time. Taken together these three components, ideal, correlated, and uncorrelated, define the conductivity behavior of the system.

## Results

In this study, two standards were used as a basis for comparison. The first is a 1M, NaCl brine in a 4 nm planar slit, and the second is a NaCl brine of various concentrations. The first standard will be used as a basis of comparison to determine the ideal range of properties for the electrode–electrolyte system. The second standard is to identify possible biases in the force-field parameters and will be compared with the concentration gradients in the slits.

**Trends in Slit Size.** As expected, the NaCl brine does not show appreciable site-specific interactions with the graphite surface. The primary effect of the surface, aside from its role as a physical barrier, is to disrupt the hydrogen-bonding network of the water, which reorganizes to minimize the energy at the interface. This process of reorganization leads to variations in the vertical profile as the interplane distance decreases (Figure 1). The peaks in the hydrogen and oxygen density profiles correspond to the structured layers that define the interfacial behavior for this system. For most of the systems examined, this structure extends out about 6–7 Å before the water in the slit behaves more like a diffuse region or bulk behavior.

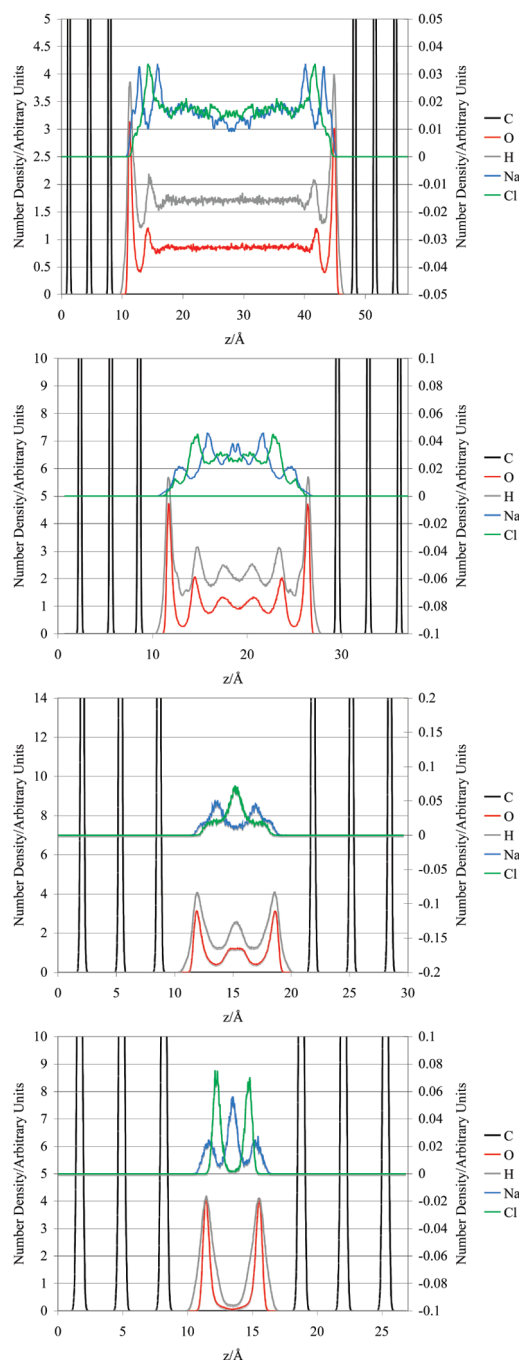


**Figure 1.** Slit pore vertical profiles. Top to bottom: 4, 2.5, 1.5, and 1 nm. Note the degree of separation of the layers in the 1.5 and 1 nm case. Because of the order-of-magnitude difference in concentration between the water and the ions, the ion values are shown on a separate axis on the right.

The vertical behavior of the ions in the system is driven by hydration. Sodium favors a position in between the oxygen peaks, while chloride favors a position within the second oxygen peak. In Figure 1 (top), it can be seen that there are two clearly defined peaks of sodium and one of chloride, a pattern that exists until confinement effects become substantial below  $\sim 2.5$  nm. For example in the 2.5 nm slit, the structured region extends a nanometer into solution from each interface fully filling the gap between carbon sheets. For the gaps smaller than 2.5 nm, the water layers begin to completely separate from one another vertically. In particular, the 1.0 nm structure does not support water structure in the center of the slit. In addition, some Na

**TABLE 3: Oxygen–Oxygen First Shell Hydration or Number of Hydrogen Bonds Per Oxygen, Na and Cl Hydration, and Na–Cl Ion Pairing Determined via Radial Distribution Numbers<sup>a</sup>**

system	O–O	Na–O	Cl–O	Cl–H	Cl–Na
1 nm slit	2.841	5.054	5.666	4.255	40.9%
1.5 nm slit	4.198	5.430	7.504	6.443	17.9%
2.5 nm slit	5.387	5.893	8.497	6.944	13.2%
4 nm slit	4.282	5.438	7.326	6.391	19.1%
4 nm slit 0.5 M	4.178	5.580	7.234	6.538	2.3%
4 nm slit 1 M	4.282	5.438	7.326	6.391	19.1%
4 nm slit 2 M	4.229	5.291	7.306	6.192	32.7%
4 nm slit 4 M	4.250	5.015	7.463	5.864	65.7%
bulk 0.5 M	4.775	5.881	7.694	6.796	1.8%
bulk 1 M	4.566	5.714	7.587	6.614	12.2%
bulk 2 M	4.599	5.563	7.676	6.474	26.8%
bulk 4 M	4.301	5.168	7.549	6.019	57.7%
1 nm nanotube	3.405	2.372	3.465	2.652	204.4%
1.5 nm nanotube	3.689	4.517	6.775	5.288	82.8%
2.5 nanotube	3.958	5.323	7.190	6.315	16.7%
3.5 Nanotube	4.210	5.461	7.353	6.409	15.4%

<sup>a</sup> All solutions 1 M unless stated otherwise.

ions do coincide with water layers, which is essentially a reversal of the ion vertical profiles observed in less confined systems. The 4 nm structure is the only slit with both diffuse and structured layers, whereas all of the other systems have only structured layers of water and ions.

The vertical behavior corresponds to patterns in water hydrogen bonding and coordination. Table 3 is generated from the integrated radial density profiles for each of the ions. The complete hydration shell for sodium is an octahedral arrangement of six waters, while the hydration shell for chloride is larger and less well-defined. The positions of the ions allow a complete hydration shell in all but the most confined system (1 nm slit) as indicated by average bonding values much less than bulk and a significant increase in ion pairing. Ion pairing is considered as a percentage of the counterions that are within a radius that corresponds to an inner-sphere coordination. Here, the reversal of the vertical profile peaks is not sufficient to provide complete hydration. There is a minimum in the ion pairing trend for the 2.5 nm slit that corresponds to an increase in the hydration of the two ions. Also in Table 3 is an estimate of water–water hydrogen bonding calculated using the oxygen–oxygen radial profiles, which shows increased interactions with respect to other sizes and bulk at 2.5 nm. The cutoff of the RDF for the oxygen oxygen distribution corresponds to the first minima in the differential RDF 3.2 Å. For bulk water, this result gives a coordination of 4.57 waters, which is slightly larger than the expected 4.0 hydrogen bonds, indicating that part of a second shell water has been included in the bulk calculation. So it can be seen that in the case of the slit, the oxygen–oxygen coordination reaches a maxima for the 2.5 nm case and is significantly larger than bulk. For the 4.0 and 1.5 nm systems, it is approximately that of bulk, and the 1.0 nm system is significantly less than bulk. This suggests that intersheet confinement of  $\sim 2.5$  nm promotes ion hydration resulting from structured layers that form at that dimension in slits. There is a dramatic increase in ion pairing for significantly confined systems. At the smallest slit size, the ion pairing increases to 40% indicating that only in the smallest 1 nm slits is there a reduction in the hydration shells of the ions. Overall, the combination of increased ion pairing and correlation means that the uncorrelated or free conductivity steadily declines in these systems as discussed below. This is a result of both

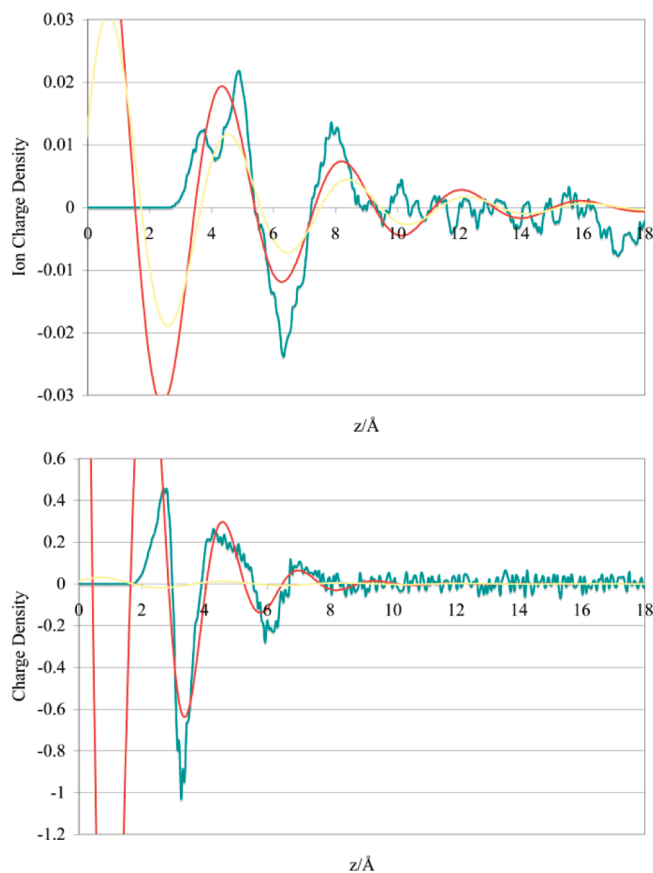


**Figure 2.** Vertical charge separation profile (teal curve) for the 1 M NaCl brine (top, NaCl ions only; bottom, water) in the 4 nm slit. The red curves are the model fit (from 3–9 Å) of the charge separation, and the yellow curves are the corresponding electrostatic potential from that model; both are taken from the differential capacitance models of Vatamanu et al.<sup>36</sup> Model parameters for the top and bottom panels are  $K = -0.058$ ,  $\lambda = 3.996$ ,  $\beta = 3.868$ ,  $\varphi = 3.801$  and  $K = 5.515$ ,  $\lambda = 1.581$ ,  $\beta = 2.415$ ,  $\varphi = 2.011$ , respectively. Distance is measured relative to the carbon surface. The misfit of the model fit to the NaCl profile is an indication of the particular nature of the aqueous double layer interface and the differences from that of an ionic liquid.

increasing confinement and increased disruption of water structure below 2.5 nm.

Differential capacitance is the measure of the change in surface charging with respect to a change in applied voltage across a capacitor. Differential capacitance is connected to the spatial offset of positive and negative charges at the interface, and models exist that describe the charge density and electrostatic potential for an ionic liquid.<sup>36</sup> We employ these models here primarily to characterize the degree of structure present in an aqueous interface, and secondarily, to connect this work to an ionic liquid interacting with a charged interface showing a similar structure and displaying differential capacitance behavior. Differences in hydration of sodium and chloride lead to an oscillatory pattern of charge balance seen in the top panel of Figure 2 ( $K = -0.058$ ,  $\lambda = 3.996$ ,  $\beta = 3.868$ ,  $\varphi = 3.801$ ). In this model, the amplitude and the phase are the parameters that would be expected to vary in response to a change in surface charge, suggesting that an increase in charge separation in an ionic liquid is what drives charge screening. In general, the model does quite well for the structured region of the interface, excluding the first shoulder of the sodium peak at  $\sim 3.5$  Å, indicating the behavior of the ions in this region is at least superficially similar to an ionic liquid. However, the model does poorly when the interface transitions into a diffuse or bulk-like

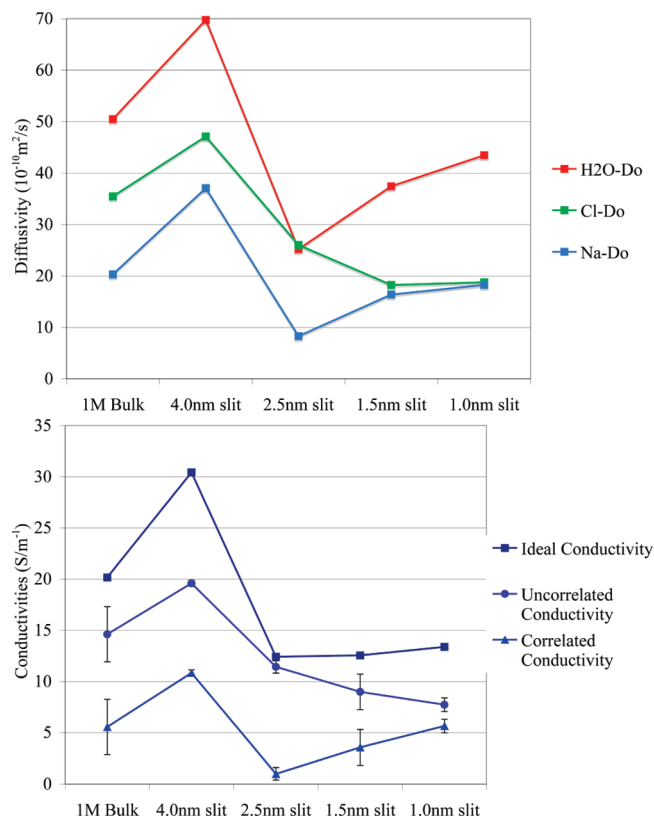


**Figure 3.** Diffusivity constants (top) and conductivities (bottom) for the slit geometries.

layer beyond  $\sim 9$  Å. As a result, while interesting in terms of the similarity between aqueous electrolytes and ionic liquids, the model is less likely to be useful as a predictor of changes in interfacial charge screening properties of aqueous sodium and chloride near charged interfaces for several reasons. First, ion hydration radii limit the ability of ions to move normal to the surface. Second, there is no capacity for this model to account for a reduction in concentration of the ion with the same charge as the surface. Finally, the amount of structure could extend further away from the surface as a result of charging. The discrepancies of the model for the aqueous interface confirms the presence of two different types of regions, a structured and a more bulk-like layer. As a result, a modification of this model is required to describe differential capacitance in an aqueous interface. Such a model would have to hybridize the different styles of behavior corresponding to the two different types of layers. Overall, it further indicates the dominant role that water plays in governing the behavior of aqueous interfaces.

Interestingly, as seen in the lower panel of Figure 2, the fit of the ionic liquid model works remarkably well for the charge separation profile for water ( $K = 5.515$ ,  $\lambda = 1.581$ ,  $\beta = 2.415$ ,  $\varphi = 2.011$ ). In this case, the model is able to fit the entire interface, not just the structured region. This result may be illustrating an unexpected similarity in the behavior of water to that of an ionic liquid at a charged interface. There is a rational basis that aids in justifying this relationship in that water can rotate to create increased separations in response to a charge, and that overall the model assumes the local environment is approximately neutral. In the fit, the phase factor is nonzero, which suggests that the minimum of differential capacitance may not be at exactly 0 V. This result is surprising but may be useful for examining interfacial structure at charged interfaces.

Figure 3 shows the diffusion profiles for the slit system. Surprisingly, the system at 4.0 nm shows enhanced diffusion

compared to bulk. This enhancement is driven by increases in the horizontal (parallel to the surface) components of the diffusion constants. For sodium and water, the horizontal components drop to a minimum at 2.5 nm but then increase again as the slit size is decreased. This increase in diffusivity following a decrease indicates that in addition to the effect of constraining the system, a second mechanism or driver must be operating. This second driver is likely to be the breakdown of water structure with ion pairing contributions, leading to the convergence of the diffusivities for chloride and sodium below 2.5 nm. We find that the diffusivity for chloride follows the general trend but does not display this global minimum at 2.5 nm, which could be a result of the diffuse nature of its hydration shell. The trends in conductivity are also shown in Figure 3. There is a distinct similarity in this graph to that of the diffusion constants. While there is an overall relationship between these curves and the diffusion constants, the likeness of the ideal conductivity to the diffusion constant for water, the uncorrelated to chloride, and the correlated to sodium is coincidental. Although there is a higher error in the correlated conductivity, its behavior still corresponds well to other properties of the system including ion hydration, water hydrogen bonding, and ion pairing. Ultimately the decline in uncorrelated conductivity from 4 to 1 nm suggests that larger slits may demonstrate better delivery properties.

**Trends in Concentration.** In general, the trend in diffusion properties as a function of concentration shows similar behavior in bulk as in the 4 nm slit (see Figure 4). The 4 nm slit was examined more closely because of the enhancement in diffusion shown in Figure 3. One exception between the slit and the bulk is the rate of diminution of the horizontal components of the diffusion coefficients, which drop off more rapidly from the maximum than in the bulk case.

As expected, ion-pairing increases dramatically as the concentration of the brine is increased, and the effect is greater in slits than in bulk (see Table 3, lines 5–12). For reference, the solubility of NaCl is approximately 6 M, so one would expect ion pairing to rise correspondingly. No other significant changes in hydration are observed as a function of concentration, but at 4 M, additional vertical structure of the ion profiles is observed, with a poorly defined third peak for sodium and a second one for chloride. This indicates saturation of available outer sphere adsorption sites.

Conductivity rises with increasing concentrations because of the dependence of the ideal conductivity on the concentration of the ions (see Figure 4). There is a clear difference in the correlated conductivity between the bulk and slit cases for moderate concentrations for the 2 ns period studied. The slit forces a much higher degree of correlation in the ions, which is not unexpected. However, it does suggest that in conjunction with the ion pairing, precipitation could occur in the slits at much lower concentrations. Furthermore, at the higher concentrations there is a limiting rate of return with respect to the ideal conductivity with increasing concentration. The fact that the ideal conductivity begins to level off at 4 M implies that it is affected by the quantity of ion pairing. Additionally, it suggests that the ion pairs move much more slowly than the free ions, and that the ideal conductivity already incorporates much of the effects of ion pairing at lower concentrations.

**Trends with Tube Size.** Although the tube constrains radially and has only one free dimension (the slit constrains one dimension with two free), the simulation results are in many respects qualitatively similar. The equivalent to vertical profiles, the normalized cylindrical profiles, are seen in Figure 5. These

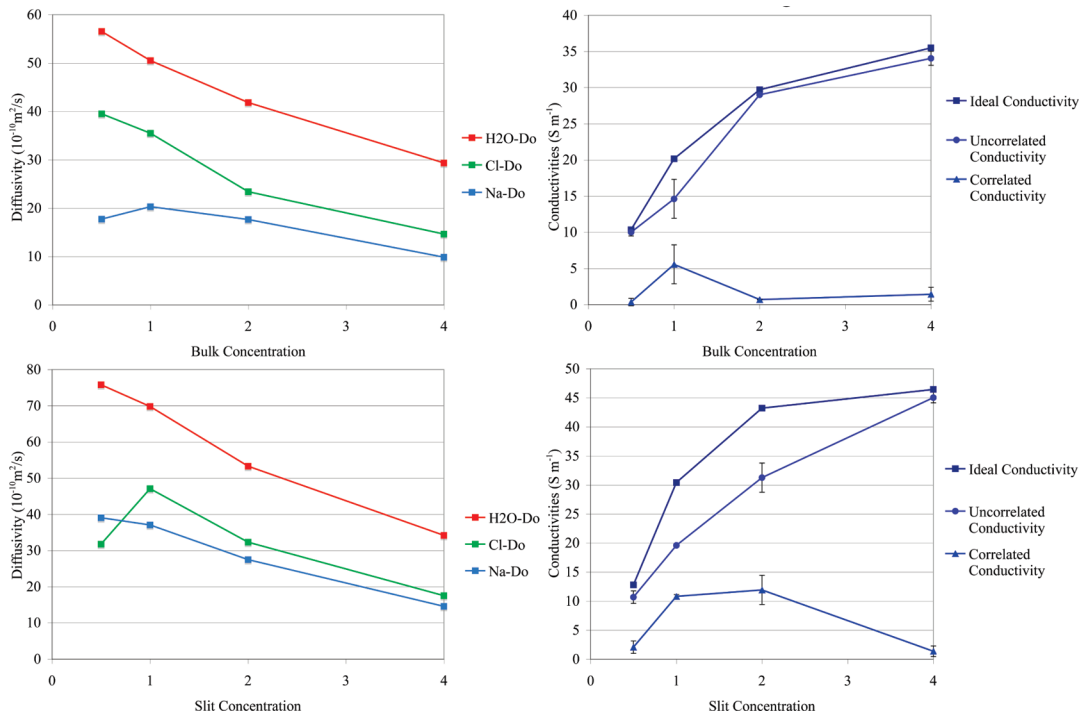


**Figure 4.** Concentration (M) effect on diffusivity and conductivity. Top: bulk (left, diffusion constants; right, conductivities). Bottom: 4 nm slit (left, diffusion constants; right, conductivities).

have been normalized by dividing by the number densities in each ring by the volume element ( $r\Delta r$ ). As in the slit case, the profiles show a clear first water peak with a weak second water peak, and there are two sodium peaks and one chloride peak upon only slight confinement. However, all the tubes show a quicker return to bulklike behavior at the center of the tube. In particular, the 2.5 nm tube shows a clearly defined diffuse layer at the center of the tube in contrast to the similar sized slit system. Unlike the slit case, there is never complete separation of the donut-shaped layers. These results suggest that the radial confinement makes it more difficult for ordered layers to form and in general promotes more bulklike behavior in the water structure. As seen in Figure 6, the diffusivities indicate slightly different behavior than the slit resulting from the change in free dimensionality. In particular, there is an initial enhancement in diffusivity upon slight confinement as before; however, there is no increase in diffusivity below 2 nm. This is despite an even stronger increase in ion pairing and decrease in hydration with decreasing tube size. The reasons for this may be the return to bulklike or diffuse behavior rather than the hyper-structured behavior observed in the 2.5 nm slit, which essentially shuts down the focused ion motion via channels parallel to the surface. Unlike the slit case, the layers appear to be much better connected. Ion pairing increases much more quickly with decreasing tube size than in the case of the slit geometry as determined from the radial distribution functions (see Table 3, last 4 lines). In particular, the ion pairing is particularly intense for the 1.0 nm tube. The value of 200% indicates that a  $\text{Na}_2\text{Cl}_2$  cluster is the dominant form of the ions in this system. Once again, the hydration of the ions is essentially complete with the exception of the smallest tube sizes.

As in the case for the slits, the conductivity is higher in the large 3.5 nm tube than in the bulk case (see Figure 6). In general however, the tubes show lower correlation than the slits. For all but the 2.5 nm tube, the correlated conductivity is within uncertainty of 0 for the 2 ns time period studied. This corresponds to a maximum in the sodium ion diffusivity. In

this case, the correlated conductivity may be responding to a balance between increasing constraints on the system and increasing ion pairing, which is driving down the ideal conductivity. The error bars for the correlated and uncorrelated conductivity overlap and so look larger than they actually are.

## Discussion

The results indicate a range of parameters useful in the design of this type of supercapacitor. For pores where the NaCl brines are fully able to infiltrate, the concentration should be maintained around 0.5 to 1 M. This range of concentrations allows for sufficient ions to promote capacitance without resulting in significant ion pairing. High ion pairing is a potential problem because ions can precipitate creating barriers within the electrode, and pairing reduces the quantity of ions available to respond freely to changes in induced potential (e.g., electrode charging). Note that the potential for ion pairing will likely decrease upon incorporating a strongly charged surface in the simulations, which is the subject of future work. Another parameter investigated was the size of the slit or cylindrical pore. For the slits, there are two different regimes of behavior, one for above 2.5 nm and one for below. While the results suggest there are reasonable diffusivities present at the smallest of the slits, high ion pairing and increasing correlation of the ions must be considered. Both of these factors work to reduce the available conductivity. For the tubes, there is a much less pronounced transition at 2.5 nm. The higher degree of constraint on the system results in much higher ion pairing. Even though the forces and global effects present in the slits and the cylindrical pores are similar, the detailed trends with decreasing dimension are notably different. Ultimately, the true pore geometry will be determined by experiment; however, it is useful to understand the types of effects that can occur in different model morphologies.

Ion pairing and hydration are competing processes that both affect ion diffusivities. In general, increased ion pairing reduces

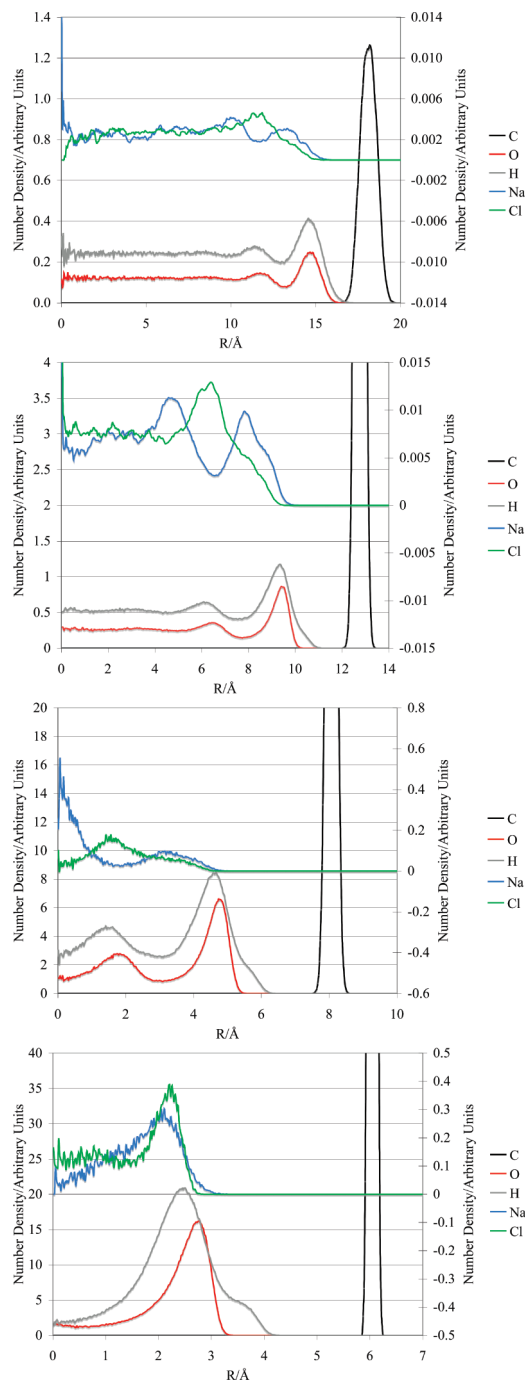


**Figure 5.** Cylindrical profiles for 1 M NaCl brines in a carbon nanotube. Top to Bottom: 3.5, 2.5, 1.5, and then 1 nm.

the diffusivity as shown in the concentration studies and in small tubes. However, significant hydrogen-bonding between heavily hydrated ions and lone water molecules can also slow ion motion as indicated by the minimum in diffusivity for 2.5 nm slits. The fact that the ion diffusivities then increase slightly upon further confining the slit system, correlating with a loss of hydrogen-bonding interactions between water molecules, further highlights the importance of hydration. In this case, the disruption of the water structure promotes increased free ion motion even though ion pairing increases under tighter confinement. This suggests that hydration drives the system dynamics and is a major contributing factor of ion diffusivities in confined systems.

It should be noted that the results presented here are a baseline for the properties under consideration in absence of an applied

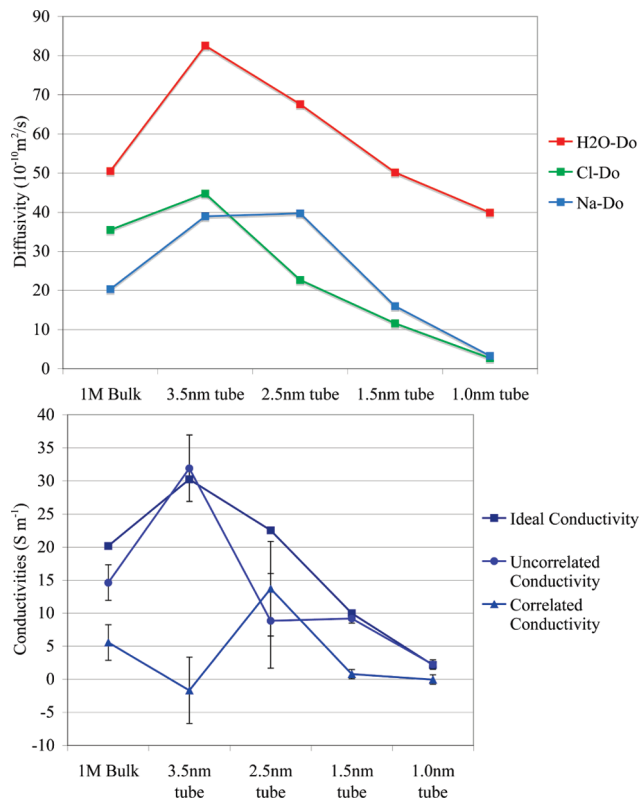


**Figure 6.** Diffusivity constants (top) and conductivities (bottom) for the cylindrical pore geometries.

voltage. Studies are currently underway to explore the effects induced upon fully charging the system.

## Conclusions

Our findings suggest that the combination of NaCl brines in contact with carbon electrodes have great potential for energy storage as a supercapacitor. In particular, systems with a moderate concentration of 0.5–1 M and slit or cylindrical pore sizes that are  $>2$  nm appear well suited to this purpose. Ions in these systems diffuse laterally, not vertically in both model systems. Hydration drives all aspects of behavior in this system including the vertical profiles, ion pairing, diffusivities, and conductivities. Water structure appears to be second most important factor in determining the system properties after the size and dimensionality of constraint on the system.

**Acknowledgment.** We are delighted to contribute this manuscript to the Festschrift celebrating the life and work of Mark A. Ratner. One of us (K.L.S.) had the pleasure of working with Mark as a postdoctoral associate. Recalling this period brings back many fond memories of the unique and wonderful environment created at Northwestern University. Mark is an exceptional scientist and more importantly a truly special person. This material is based upon work supported as part of the Fluid Interface Reactions, Structures, and Transport (FIRST) Center, an Energy Frontier Research Center funded by the U.S. Department of Energy, Office of Science, and Office of Basic Energy Sciences under Award Number ERKCC61. K.L.S. thanks Drexel University for startup funding, which purchased the computer cluster used for these calculations.

## References and Notes

- (1) Conway, B. E. *Electrochemical Supercapacitors: Scientific Fundamentals and Technological Applications*; Plenum: New York, 1999.

- (2) Barsukov, I. V.; Johnson, C. S.; Doninger, J. E.; Barsukov, V. Z. *New Carbon Based Materials for Electrochemical Energy Storage Systems: Batteries, Supercapacitors and Fuel Cells*; Springer: Netherlands, 2006.
- (3) Frackowiak, E. *Phys. Chem. Chem. Phys.* **2007**, *9*, 1774.
- (4) Arico, A. S.; Bruce, P.; Scrosati, B.; Tarascon, J.-M.; Schalkwijk, W. v. *Nat. Mater.* **2005**, *4*, 368.
- (5) Pandolfo, A. G.; Hollenkamp, A. F. *J. Power Sources* **2006**, *157*, 11.
- (6) Winter, M.; Brodd, R. J. *Chem. Rev.* **2004**, *104*, 4245.
- (7) Kotz, R.; Carlen, M. *Electrochim. Acta* **2000**, *45*, 2483.
- (8) Sarangapani, S.; Tilak, B. V.; Chen, C.-P. *J. Electrochem. Soc.* **1996**, *143*, 3791.
- (9) Liu, L.; Zhao, J.; Yin, C.-Y.; Culligan, P. J.; Chen, X. Mechanisms of water infiltration into conical hydrophobic nanopores. *Phys. Chem. Chem. Phys.* **2009**, *11*, 6520–6524.
- (10) Simon, P.; Gogotsi, Y. Materials for electrochemical capacitors. *Nat. Mater.* **2008**, *7*, 844–893.
- (11) Huang, J.; Sumpter, B. G.; Meunier, V. Theoretical Model for Nanoporous Carbon Supercapacitors. *Angew. Chem. Int. Ed.* **2008**, *47*, 520–524.
- (12) Zhao, J.; Culligan, P. J.; Germaine, J. T.; Chen, X. Experimental Study on Energy Dissipation of Electrolytes in Nanopores. *Langmuir* **2009**, *25* (21), 12687–12696.
- (13) Largeot, C.; Portet, C.; Chmiola, J.; Taberna, P.-L.; Gogotsi, Y.; Simon, P. Relation between the Ion Size and Pore Size for an Electric Double-Layer Capacitor. *J. Am. Chem. Soc.* **2008**, *130*, 2730–2731.
- (14) Chmiola, J.; Yushin, G.; Gogotsi, Y.; Portet, C.; Simon, P.; Taberna, P. L. Sizes Less Than 1 Nanometer. *Science* **2006**, *313*, 1760–1763.
- (15) Shim, Y.; Kim, H. J. Nanoporous Carbon Supercapacitors in an Ionic Liquid: A Computer Simulation Study. *ACS Nano* **2010**, *4* (4), 2345–2355.
- (16) Goodenough, J. B.; Abruna, H. D.; Buchanan, M. V. Basic Research Needs for Electrical Energy Storage: Report of the Basic Energy Sciences Workshop for Electrical Energy Storage. In *Sciences*, Department of Energy: Washington, DC, 2007; p 186.
- (17) Kotz, R.; Carlen, M. Principles and applications of electrochemical capacitors. *Electrochim. Acta* **2000**, *45*, 2483–2498.
- (18) Tang, W.; Advani, S. G. Non-equilibrium molecular dynamics simulation of water flow around a carbon nanotube. *Comput. Model. Simul. Eng. Sci.* **2007**, *22* (1), 31–40.
- (19) (a) Liu, L.; Zhao, J.; Culligan, P. J.; Qiao, Y.; Chen, X. Thermally Responsive Fluid Behaviors in Hydrophobic Nanopores. *Langmuir* **2009**, *25* (19), 11862–11868. (b) Liu, L.; Zhao, J.; Culligan, P. J.; Qiao, Y.; Chen, X. *Langmuir* **2009**, *25* (19), 11862–11868.
- (20) Liu, L.; Chen, X.; Lu, W.; Han, A.; Qiao, Y. Infiltration of Electrolytes in Molecular-Sized Nanopores. *Phys. Rev. Lett.* **2009**, *102*, 184501–184504.
- (21) Vaitheeswaran, S.; Reddy, G.; Thirumalai, D. Water-mediated interactions between hydrophobic and ionic species in cylindrical nanopores. *J. Chem. Phys.* **2009**, *130*, 094502.
- (22) Zuo, G.; Shen, R.; Ma, S.; Guo, W. Transport Properties of Single-File Water Molecules inside a Carbon Nanotube Biomimicking Water Channel. *ACS Nano* **2010**, *4* (1), 205–210.
- (23) Ohba, T.; Kanoh, H.; Kaneko, K. Structures and Stability of Water Nanoclusters in Hydrophobic Nanospaces. *Nano Lett.* **2005**, *5* (2), 227–230.
- (24) Mukherjee, B.; Maiti, P. K.; Dasgupta, C.; Sood, A. K. Single-File Diffusion of Water Inside Narrow Carbon Nanorings. *ACS Nano* **2010**, *4* (2), 985–991.
- (25) Nicholson, D.; Quirke, N. Ion pairing in confined electrolytes. *Mol. Simul.* **2003**, *29* (4), 287–290.
- (26) Di Leo, J. M.; Maranon, J. Cation transport in nanopores. *Mol. Simul.* **2009**, *35* (4), 280–286.
- (27) Leung, K. Ion Rejection by Nanoporous Membranes in Pressure-Driven Molecular Dynamics Simulations. *J. Comput. Theor. Nanosci.* **2009**, *6* (8), 1948.
- (28) Argyris, D.; Cole, D. R.; Striolo, A. Ion-Specific Effects under Confinement: The Role of Interfacial Water. *ACS Nano* **2010**, *4* (4), 2035–2042.
- (29) Shirono, K.; Tatsumi, N.; Daiguji, H. Molecular Simulation of Ion Transport in Silica Nanopores. *J. Phys. Chem. B* **2009**, *113*, 1041–1047.
- (30) Coppens, M.-O.; Dammers, A. J. Effects of heterogeneity on diffusion in nanopores—From inorganic materials to protein crystals and ion channels. *Fluid Phase Equilib.* **2006**, *241*, 308–316.
- (31) Lamperski, S.; Outhwaite, C. W.; Bhuiyan, L. B. The Electric Double-Layer Differential Capacitance at and near Zero Surface Charge for a Restricted Primitive Model Electrolyte. *J. Phys. Chem. B* **2009**, *113*, 8925–8929.
- (32) Feng, G.; Qiao, R.; Huang, J.; Sumpter, B. G.; Meunier, V. Ion Distribution in Electrified Micropores and Its Role in the Anomalous Enhancement of Capacitance. *ACS Nano* **2010**, *4* (4), 2382–2391.
- (33) Plimpton, S. J. Fast Parallel Algorithms for Short-Range Molecular Dynamics. *J. Comp. Phys.* **1995**, *117*, 1–19.
- (34) Plimpton, J.; Pollock, R.; Stevens, M. In *Particle-Mesh Ewald and rRESPA for Parallel Molecular Dynamics Simulations*, Proceedings of the Eighth SIAM Conference on Parallel Processing for Scientific PPSC 1997, March 14–17, Minneapolis, MN, 1997.
- (35) *Accelrys Materials Studio*. Accelrys Software Inc.: San Diego, CA, 2001–2007.
- (36) Vatamanu, J.; Borodin, O.; Smith, G. D. Molecular dynamics simulations of atomically flat and nanoporous electrodes with a molten salt electrolyte. *Phys. Chem. Chem. Phys.* **2010**, *12*, 170–182.
- (37) Cygan, R. T.; Liang, J.-J.; Kalinichev, A. G. Molecular Models of Hydroxide, Oxyhydroxide, and Clay Phases and the Development of a General Force Field. *J. Phys. Chem. B* **2004**.
- (38) Weiner, S. J.; Kollman, P. A.; Case, D. A.; Singh, U. C.; Ghio, C.; Alagona, G.; Profeta, S.; Weiner, P. A new force field for molecular mechanical simulation of nucleic acids and proteins. *J. Am. Chem. Soc.* **1984**, *106* (3), 765–784.
- (39) Kalinichev, A. Michigan State University. Personal communication, 2006.
- (40) Borodin, O. Polarizable Force Field Development and Molecular Dynamics Simulations of Ionic Liquids. *J. Phys. Chem. B* **2009**, *113*, 11463–11478.